Rainforest-like Atmospheric Chemistry in a Polluted Megacity

Mike J. Newland[1], Daniel J. Bryant[1], Rachel E. Dunmore[1], Thomas J. Bannan[2], W. Joe F. Acton[3], Ben Langford[4], James R. Hopkins[1,5], Freya A. Squires[1], William Dixon[1], William S. Drysdale[1], Peter D. Ivatt[1], Mathew J. Evans[1], Peter M. Edwards[1], Lisa K. Whalley[6,7], Dwayne E. Heard[6,7], Eloise J. Slater[6], Robert Woodward-Massey[8], Chunxiang Ye[8], Archit Mehra[2], Stephen D. Worrall[2,a], Asan Bacak[2], Hugh Coe[2], Carl J. Percival[2,b], C. Nicholas Hewitt[3], James D. Lee[1,5], Tianqu Cui[9], Jason D. Surratt[9], Xinming Wang[10], Alastair C. Lewis[1,5], Andrew R. Rickard[1,5], Jacqueline F. Hamilton[1]

[1]Wolfson Atmospheric Chemistry Laboratories, Department of Chemistry, University of York, York, UK
[2]School of Earth and Environmental Sciences, The University of Manchester, Manchester, UK
[3]Lancaster Environment Centre, Lancaster University, Lancaster, UK
[4]Centre for Ecology and Hydrology, Edinburgh, EH26 0QB, UK
[5]National Centre for Atmospheric Science (NCAS), University of York, York, UK
[6]School of Chemistry, University of Leeds, Leeds, UK
[7]National Centre for Atmospheric Science, School of Chemistry, University of Leeds, UK
[8]Beijing Innovation Center for Engineering Science and Advanced Technology, State Key Joint Laboratory for Environmental Simulation and Pollution Control, Center for Environment and Health, College of Environmental Sciences and Engineering, Peking University, Beijing, 100871, China
[9]Department of Environmental Sciences and Engineering, Gillings School of Global Health, University of North Carolina, Chapel Hill, USA
School of Engineering and Applied Science, Aston University, Birmingham, UK
[10]Guangzhou Institute of Geochemistry, Chinese Academy of Sciences, Guangzhou, China
[a]now at: Chemical Engineering and Applied Chemistry, School of Engineering and Applied Science, Aston University, Birmingham, UK
[b]now at: Jet Propulsion Laboratory, California Institute of Technology, 4800 Oak Grove Drive, Pasadena, CA, USA

Correspondence to: Mike J. Newland (mike.newland@york.ac.uk)
Jacqueline F. Hamilton (Jacqui.hamilton@york.ac.uk)

Abstract. The impact of volatile organic compound (VOC) emissions to the atmosphere on the production of secondary pollutants, such as ozone and secondary organic aerosol (SOA), is mediated by the concentration of nitric oxide (NO). Polluted urban atmospheres are typically considered to be "high-NO" environments, while remote regions such as rainforests, with minimal anthropogenic influences, are considered to be "low-NO". Policy to reduce urban air pollution is typically developed assuming that the chemistry is controlled by the high-NO regime. However, our observations from central Beijing show that this simplistic separation of regimes is flawed. Despite being in one of the largest megacities in the world, we observe significant formation of gas and aerosol phase oxidation products associated with the low-NO 'rainforest-like' regime during the afternoon. This is caused by a surprisingly low concentration of NO, coupled with high concentrations of VOCs and of the atmospheric oxidant hydroxyl (OH). Box model calculations suggest that during the morning high-NO chemistry predominates (95%) but in the afternoon low-NO chemistry plays a greater role (30%). With increasing global emphasis on reducing air pollution, the modelling tools used to develop urban air quality policy need to adequately represent both high- and low-NO regimes if they are to have utility.

1 Introduction

The atmosphere in polluted urban areas has a markedly different chemical composition to that in remote regions (e.g. rainforests). This can lead to changes in the chemical oxidation pathways for volatile organic compounds (VOCs), giving rise to the formation of different secondary pollutants. Oxidation by hydroxyl radicals (OH) is the dominant daytime sink for VOCs, leading to the formation of highly reactive peroxy radicals (RO_2). In atmospheres with high concentrations of nitric oxide (NO), emitted by combustion sources such as vehicles, cooking, and energy generation, RO_2 radicals react predominantly with NO (Orlando and Tyndall, 2012). This tends to break the initial VOC down to smaller, more oxidised VOCs, and can also produce organic nitrates ($RONO_2$). This pathway also produces NO_2, the photolysis of which leads to ozone production. In contrast, in low-NO atmospheres RO_2 predominantly react with other RO_2, including hydroperoxyl radicals (HO_2), or can isomerize/auto-oxidise to form different multi-functionalized oxygenated RO_2 (Crounse et al., 2013). These low NO pathways tend to maintain the original carbon skeleton. The large highly oxidised molecules formed can efficiently partition to the aerosol phase to yield secondary organic aerosol (SOA) (Bianchi et al., 2019), which often comprises a large fraction of submicron atmospheric particulate matter (PM) in many regions (Jimenez et al., 2009).

Biogenic sources dominate global emissions of VOCs to the atmosphere, with the highly reactive VOC isoprene (2-methyl-1,3-butadiene) contributing ~70% by mass (Sindelarova et al., 2014). The gas and aerosol phase products of isoprene oxidation have been extensively characterized in the laboratory (Wennberg et al., 2018). In this work a range of isoprene oxidation products are used as tracers of the changing atmospheric chemical environment. For isoprene, the low-NO oxidation pathway leads to low volatility products, such as isoprene hydroperoxides (ISOPOOH), that can go on to form significant quantities of SOA via formation of isoprene epoxides (IEPOX) (Figure 1) (Paulot et al., 2009; Surratt et al., 2010; Lin et al., 2012). The high-NO pathway can also form SOA via the formation of methacrolein (MACR), which can react further to form SOA constituents such as 2-methylglyceric acid (2-MGA) and corresponding oligomers (Kroll et al., 2006; Surratt et al., 2006; 2010; Nguyen et al., 2015) (Figure 1). Other significant contributors to isoprene-SOA formed via the high NO pathway include nitrates (e.g. $ISOPONO_2$) and dinitrates (Schwantes et al., 2019).

2 Results

Beijing is a megacity (population of 21.4 M) with an atmospheric reactive VOC mix with both biogenic and anthropogenic influences. Mean diurnal cycles of ozone, NO, isoprene, and a range of gas and aerosol phase isoprene oxidation products measured at a city-centre site in summer 2017 (Shi et al., 2019) are shown in Figure 2. Ozone increases throughout the day to a mid-afternoon peak (Figure 2a), driven by the photolysis of NO_2, which is rapidly regenerated through the reactions of ozone, RO_2 and HO_2 with NO. The high level of ozone acts to suppress NO concentrations. Such a diurnal cycle is typical of urban environments (Ren et al., 2003; Whalley et al., 2018). However, ozone is so high in Beijing, with mixing ratios regularly >100

ppbv in the afternoon, that on many days NO concentrations fall to < 0.5 ppbv in the afternoon, and on some days to < 0.1 ppbv (see Supplementary Information).

The observed diurnal cycles of 'low-NO' and 'high-NO' isoprene oxidation products (Figure 1) in both the gas and aerosol phases can be explained by the observed diurnal cycle of NO (Figure 2a). The high-NO product isoprene nitrate (ISOPONO$_2$) (Figure 2c) is produced through the morning from reaction of isoprene peroxy radicals (ISOPOO) with NO. During the afternoon, an increasing fraction of ISOPOO begins to react with HO$_2$ or RO$_2$ as the NO concentration drops. This leads to the observed decrease in ISOPONO$_2$, and an increase in IEPOX + ISOPOOH through the afternoon (Figure 2b). The profile of the high-NO products MACR+MVK (Figure 2d) is very similar to that of ISOPONO$_2$ until about 15:00, when they begin to increase, with a second peak observed at around 17:00. This latter peak may be an observational artefact as a result of the conversion of ISOPOOH to MACR on metal surfaces within the inlet of the PTR instrument (Rivera-Rios et al., 2014). Isoprene oxidation products can also partition into the particle phase and undergo heterogeneous reactions to form organosulfates, with concentrations driven by a number of additional factors such as particulate sulfate and water vapour concentrations. Specific organosulfate tracers from the high-NO (2-MGA-OS, Figure 2e) and low-NO (2-methyltetrol-OS formed from IEPOX, Figure 2f) pathways were observed, with low concentrations overnight, increasing during the day to a peak around 15:00-16:00.

The observed temporal profiles of the isoprene tracer products suggest a chemical cycle switching from a high-NO to a low-NO chemical regime during the day in Beijing. First, isoprene nitrates, formed predominantly during the morning (Figure 2c), are characteristic of high-NO chemistry. Second, isoprene hydroperoxides (ISOPOOH) and epoxydiols (IEPOX) (Figure 2b), formed predominantly during the afternoon, are characteristic of low-NO chemistry, where the reaction of ISOPOO with HO$_2$ dominates over reaction with NO. The formation of highly oxygenated molecules (HOMs), characteristic of RO$_2$ isomerisation and auto-oxidation in low NO environments, has also been observed during the afternoon at this site (Brean et al., 2019). Third, the observation of large amounts of 2-methylglyceric acid (2-MGA-OS) (Figure 2e) in the aerosol is suggestive of both high and low NO chemistry having occurred. The precursor to 2-MGA, methacrolein (MACR), is formed predominantly via reactions of ISOPOO with NO (Figure 1), i.e. during the morning. In the afternoon, the RO$_2$ formed from oxidation of MACR reacts with NO$_2$ (in preference to NO, because of the very low NO/NO$_2$ ratio) and further oxidation leads to 2-MGA (Surratt et al., 2010; Chan et al., 2010; Nguyen et al., 2015).

3 Box Modeling

The chemical box model DSMACC (Emmerson and Evans, 2009), coupled with the near-explicit oxidation mechanism for isoprene from the Master Chemical Mechanism (MCM v3.3.1) (Jenkin et al., 1997; 2015), was used to assess the sensitivity of the fraction of ISOPOO reacting with NO (f_{NO}) to varying NO concentrations and the OH reactivity ($\sum k_{OH+VOC}$ [VOC]). The model was run to steady state at a range of different fixed concentrations of [OH], [NO], and [isoprene], using fixed photolysis rates typical of Beijing daytime (see Supplementary Information). Figure 3 shows that, as expected, f_{NO} increases

with increasing NO concentration. It also shows that f_{NO} is not a fixed value for a given concentration of NO, but decreases
105 with the increasing reactivity of the system (the x-axis in Figure 3). The reactivity varies as a function of the VOC mixing
ratios, the reactive mix of VOCs, and the OH concentration, i.e. [OH] x OH reactivity* (Equation E1). This term effectively
defines the rate of production of RO_2. Higher reactivity and higher OH concentrations both lead to a higher concentration of
peroxy radicals ($[HO_2] + \sum[RO_2]$), reducing f_{NO}. Average measurements of ($[OH] \times$ OH reactivity*) and [NO] for the afternoon
(12:00 – 20:00) from a range of different environments are shown in Figure 3 (see also Table S1). The RO_2 chemistry in the
110 rural southeastern US and the Borneo rainforest lies in the low NO regime (i.e. $f_{NO} < 0.5$) for the whole afternoon. In the urban
areas of London and New York the chemistry remains in the high NO regime through the whole afternoon. However, in
Beijing, the extreme suppression of NO concentrations in the afternoon drives the chemistry from a regime in which > 95 %
of the RO_2 is reacting with NO during the morning, to one in which less than 70 % is reacting with NO by mid-afternoon.

4 Discussion and Conclusions

115 The major driver of the very low afternoon NO mixing ratios is the high levels of ozone. However, model runs with the regional
chemical transport model GEOS-Chem show that the low NO levels cannot be explained solely through suppression by ozone
using current understanding of atmospheric chemistry (Supplementary Information). One explanation may be additional NO
sinks that recycle OH without producing O_3 which have previously been proposed for the high VOC-low NO (< 1ppbv)
conditions seen in Beijing and other cities (Hofzumahaus et al., 2009; Whalley et al., 2018; Tan et al., 2019). Another
120 explanation may be the presence of high concentrations of other species that can convert NO to NO_2 e.g. halogen oxides. The
failure of regional and global models to accurately replicate this chemistry has wider implications for the prediction of
secondary pollutants and hence for determining policies to control air pollution episodes.

Our observations from Beijing challenge the commonly accepted view of polluted urban areas as high-NO atmospheric
125 environments in two ways. First, very high ozone regularly reduces afternoon NO to < 1ppbv, and on some days to < 0.1 ppbv.
This leads to the formation of 'low-NO' products in the gas and aerosol phase. Second, the level of NO that is required for
'low-NO chemistry' to occur is not a fixed value, but is dependent on the concentration and reactivity of the VOCs present
and the concentration of OH. Hence NO concentrations that represent 'low-NO' conditions in a tropical rainforest, for example,
are different to those that represent 'low-NO' conditions in a highly polluted urban environment with elevated VOC/OH
130 reactivity.

Under the conditions observed in Beijing, the production of low-NO SOA and the associated increase in PM is shown to be
closely linked to photochemical ozone production. Policies that reduce the afternoon ozone peak might also be expected to
reduce the production of these aerosol-phase products. However, such policies must also take account of the complex
135 interactions between NO_x, VOCs, ozone, and PM. For example, reducing NO_x emissions can counter-intuitively lead to

increases in ozone, as has occurred in other major cities (Air Quality Expert Group, 2009), while reducing PM has also been shown to lead to increases in ozone (Jacob et al., 2019). With many existing and developing megacities being located in subtropical regions with high emissions of reactive biogenic VOCs, and with the continued and increasing use of fossil fuels for transport and power generation, such extreme chemical environments as that observed in Beijing can be expected to

140   proliferate. In these environments, biogenic emissions of isoprene can dominate the OH reactivity making reduction of VOC reactivity through emissions controls very difficult. Additionally, since many Asian megacities are situated within much larger densely populated regions, attempts to control air quality are likely to be ineffective unless implemented on a regional scale. Identification of the best policy for a particular city-region will require detailed atmospheric chemical modelling with chemical mechanisms capable of simulating the appropriate chemical environments both for the present day and for future environments.

145

Methods

The site was located at the Institute of Atmospheric Physics, between the 3rd and 4th ring road. Measurements took place between 17/05/2017 and 24/06/2017. The site is typical of central Beijing, surrounded by residential and commercial properties and is near several busy roads. It is also close to several green spaces, including a tree-lined canal to the south and the Olympic

150   forest park to the north-east. Isoprene mixing ratios were measured by dual channel gas chromatography (DC-GC-FID). IEPOX/ISOPOOH were observed using iodide chemical ionisation mass spectrometry. The sum of MACR + MVK was measured using proton transfer mass spectrometry. Particle samples were collected onto filter papers at either 3 hourly or 1 hourly time periods, depending on pollution levels. Filters were extracted and analysed with a high throughput method using ultra high-pressure liquid chromatography coupled to a Q-Exactive Orbitrap mass spectrometer. Nitric oxide, NO, was

155   measured by chemiluminescence with a Thermo Scientific Model 42i NO$_x$ analyser. Nitrogen dioxide, NO$_2$, was measured using a Teledyne Model T500U Cavity Attenuated Phase Shift (CAPS) spectrometer. Ozone, O$_3$, was measured using a Thermo Scientific Model 49i UV photometer.

DC-GC-FID

160   Observations of VOCs were made using a dual-channel GC with flame ionisation detectors. Air was sampled at 30 L min^{-1} at a height of 5m, through a stainless-steel manifold (½" internal diameter). 500 mL subsamples were taken, dried using a glass condensation finger held at -40°C and then pre-concentrated using a Markes Unity2 pre-concentrator on a multi-bed Ozone Precursor adsorbent trap (Markes International Ltd). These samples were then transferred to the GC oven for analysis following methods described by Hopkins et al (2011).

165

CIMS

A time of fight chemical ionisation mass spectrometer (ToF-CIMS) (Lee et al., 2014; Priestley et al., 2018) using an iodide ionisation system was couple deployed here. Experimental set up of the University of Manchester ToF-CIMS has been previously described in Zhou et al. (2019). During the campaign, gas phase backgrounds were established through regularly

overflowing the inlet with dry N_2 for 5 continuous minutes every 45 minutes and were applied consecutively. The overflowing of dry N_2 will have a small effect on the sensitivity of the instrument to those compounds whose detection is water dependent. Here we find that due to the very low instrumental background for $C_5H_{10}O_3$ and $C_5H_9NO_4$, the absolute error remains small from this effect (<10 ppt in both reported measurements).

Field calibrations were regularly carried out using known concentration formic acid gas mixtures made in a custom-made gas phase manifold. A range of other species were calibrated for after the campaign, and relative calibration factors were derived using the measured formic acid sensitivity during these calibrations, as has been performed previously (Le Breton et al. 2018, Bannan et al. 2015). In addition to this, offline calibrations, prior to and after the field work project, of a wide range of organic acids, HNO_3 and Cl_2 were performed to assess possible large scale sensitivity changes over the measurement period. No significant changes were observed. Offline calibrations after the field work campaign were performed specific to the isoprene oxidation species observed here. IEPOX ($C_5H_{10}O_3$) synthesized by the University of North Carolina, Department of Environmental Sciences & Engineering was specifically calibrated for here. Aliquots of known concentrations of IEPOX ($C_5H_{10}O_3$) were thermally desorbed into a known continuous flow of nitrogen. For $C_5H_9NO_4$ there was no direct calibration source available and concentrations using the calibration factor of $C_5H_{10}O_3$ are presented here.

PTR-MS

A Proton Transfer Reaction-Time of Flight-Mass Spectrometer (PTR-ToF-MS 2000, Ionicon Analytik GmBH, Innsbruck) was deployed at the base of the 325m meteorological tower at the IAP field site. This instrument has been described in detail by Jordan et al. (2009). The PTR-ToF-MS was operated at a measurement frequency of 5 Hz and an E/N ratio (where E represents the electric field strength and N the buffer gas density) in the drift tube of 130 Td. To enable accurate calibration of the mass scale trichlorobenzene was introduced by diffusion into the inlet stream.

The instrument was switched between two inlet systems in an hourly cycle. For the first 20 minutes of each hour, the PTR-MS sampled from a gradient switching manifold and for the next 40 minutes, the instrument subsampled a common flux inlet line running from the 102m platform on the tower to the container in which the PTR-ToF-MS was housed. Gradient measurements were made from 3, 15, 32, 64 and 102 m with air sampled down 0.25 inch O.D. PFA lines and split between a 3 L min^{-1} bypass and 300 ml min^{-1} sample drawn to a 10 L stainless steel container. During the gradient sampling period, the PTR-ToF-MS subsampled for 2 minutes from each container giving an hourly average concentration at each height. In this work, only data from the 3m gradient height is discussed.

Zero air was generated using a platinum catalyst heated to 260 °C and was sampled hourly in the gradient switching cycle. During the field campaign, the instrument was calibrated twice weekly using a 15 component 1 ppmv VOC standard (National Physical Laboratory, Teddington). The calibration gas flow was dynamically diluted into zero air to give a six-point calibration. Data was analysed using PTR-MS Viewer 3.

PM$_{2.5}$ filter sampling and analysis

205 PM$_{2.5}$ filter samples were collected using an ECOTECH HiVol 3000 (Ecotech, Australia) high volume air sampler with a selective PM$_{2.5}$ inlet, with a flow rate of 1.33 m^3 min^{-1}. Filters were baked at 500 °C for five hours before use. After collection, samples were wrapped in foil, and then stored at -20 °C and shipped to the laboratory. Samples were collected at a height of 8 m, on top of a building in the IAP complex. Hourly samples were taken on 11th June between 08:00-17:00, with one further sample taken overnight. The extraction of the organic aerosol from the filter samples was based on the method of Hamilton et

210 al. (2008). Initially, roughly an 8th of the filter was cut up into 1 cm^2 pieces. 4 ml of LC-MS grade H$_2$O was then added to the sample and left for two hours. The samples were then sonicated for 30 minutes. Using a 2 ml syringe, the water extract is then pushed through a 0.22µm filter (Millipore) into another sample vial. An addition 1 mL of water was added to the filter sample, then extracted through the filter, to give a combined aqueous extract. This extract was then reduced to dryness using a vacuum solvent evaporator (Biotage, Sweden). The dry sample was then reconstituted in 1 mL 50:50 MeOH:H$_2$O solution, ready for

215 analysis.

The extracted filter samples and standards were analysed using UPLC-MS^2, using an Ultimate 3000 UPLC (Thermo Scientific, USA) coupled to a Q-exactive Orbitrap MS (Thermo Fisher Scientific, USA) with a heated electrospray ionisation (HESI). The UPLC method uses a reverse phase 5 µm, 4.6 x 100mm, Accucore column (Thermo scientifc, UK) held at 40 °C. The mobile phase consists of LC-MS grade water and 100 % MeOH (Fisher Chemical, USA). The water was acidified using 0.1

220 % formic acid to improve peak resolution. The injection volume was 2 µl. The solvent gradient was held for a minute at 90:10 H$_2$O:MeOH, the gradient then changed linearly to 10:90 H$_2$O:MeOH over 9 minutes, it was then held for 2 minutes at this gradient before returning to 90:10 H$_2$O:MeOH over 2 minutes and then held at 90:10 for the remaining 2 minutes, with a flow rate of 300 µL min^{-1}. The mass spectrometer was operated in negative mode using full scan MS^2. The electrospray voltage was 4.00 kV, with capillary and auxiliary gas temperatures of 320 °C. The scan range was set between 50 - 750 m/z. Organosulfates

225 were quantified using an authentic standard of 2-MGA-OS obtained from J. Surratt using the method in Bryant et al. (2019).

OH measurements

The OH radical measurements were made from the roof of the University of Leeds FAGE instrument container at the IAP field site. Two Fluorescence Assay by Gas Expansion (FAGE) detection cells where housed in a weather-proof enclosure at a

230 sampling height of approximately 4 m. OH and HO$_2$ radicals were detected sequentially in the first cell (the HO$_x$ cell), whilst HO$_2$* and total RO$_2$ radical observations were made using the second FAGE cell (the RO$_x$ cell) which was coupled with a flow reactor to facilitate RO$_2$ detection (Whalley et al., 2018). A Nd:YAG pumped Ti:Sapphire laser was used to generate 5 kHz pulsed tunable UV light at 308 nm and used to excite OH via the Q1(1) transition of the $\mathbf{A^2\Sigma^+, v' = 0 \leftarrow X^2\Pi_i, v'' = 0}$ band. On-resonance fluorescence was detected using a gated micro-channel plate photomultiplier and photon counting. A

235 background signal from laser and solar scatter and detector noise was determined by scanning the laser wavelength away from the OH transition (OHWAVE-BKD). For the entire campaign, the HO$_x$ cell was equipped with an inlet pre injector (IPI) which chemically scavenged ambient OH by periodically by injecting propane into the air stream just above the FAGE inlet. The

removal of ambient OH by chemical reaction provided an alternative means to determine the background signal (OH$_{CHEM-BKD}$),
without the need to tune the laser wavelength. By comparison with OH$_{WAVE-BKD}$, OH$_{CHEM-BKD}$ was used to identify if any OH

240 was generated internally within the FAGE cell, acting as an interference signal. In general, good agreement between OH$_{CHEM-}$
$_{BKD}$ and OH$_{WAVE-BKD}$ was observed, with a ratio of 1.07 for the whole campaign (Woodward-Massey, 2018). In this paper, the
OH$_{CHEM}$ observations are used. The instrument was calibrated every few days by over-flowing the detection cell inlet with a
turbulent flow of high purity humid air containing a known concentration of OH (and HO$_2$) radicals generated by photolysing
a known concentration of H$_2$O vapour at 185 nm. The product of the photon flux at 185 nm and the time spent in the photolysis

245 region was measured before and after the campaign using N$_2$O actinometry (Commane et al., 2010).

OH reactivity measurements

OH reactivity measurements were made using a laser flash photolysis pump-probe technique (Stone et al., 2016). Ambient air,
sampled from the roof of the FAGE container, was drawn into a reaction cell at a flow rate of 15 SLM. A 1 SLM flow of high

250 purity, humidified air which had passed by a Hg lamp, generating ~50 ppbv of ozone, was mixed with the ambient air at the
entrance to the reaction cell. The ozone present was photolysed by 266 nm laser light at a pulse repetition frequency of 1 Hz
along the central axis of the reaction cell, leading to the generation of a uniform profile of OH radicals following the reaction
of O(^{1}D) with H$_2$O vapour. The decay in the OH radical concentration by reaction with species present in the ambient air was
monitored by sampling a portion of the air into a FAGE cell positioned at the end of the reaction cell. A fraction of the 5 kHz,

255 308 nm radiation generated by the Ti:Sapphire laser, passed through the OH reactivity FAGE cell, perpendicular to the air
stream, electronically exciting the OH radicals and the subsequent laser-induced fluorescence signal was detected with a gated
channel photomultiplier tube. The 1 Hz OH decay profiles were integrated for 5 minutes and fitted to a first-order rate equation
to determine the observed loss rate of OH (k$_{obs}$). The total OH reactivity, k(OH), was calculated by subtracting the rate
coefficient associated with physical losses of OH (k$_{phys}$) from k$_{obs}$. k$_{phys}$ was determined by monitoring the decay of OH when

260 the ambient air was replaced with a flow of 15 SLM high purity air. A small correction to account for dilution of the ambient
air by the 1 SLM flow of ozone-containing synthetic air was also applied.

Box Modelling

The box modelling that feeds into Figure 3 was performed using the Dynamically Simple Model of Atmospheric Chemical

265 Complexity (DSMACC), zero-dimensional box model (Emmerson and Evans, 2009), together with the isoprene scheme,
together with the relevant inorganic chemistry, from the near explicit chemical mechanism the Master Chemical Mechanism
(MCM) v3.3.1 (Jenkin et al., 1997; Jenkin et al., 2015). The complete isoprene degradation mechanism in MCM v3.3.1 consists
of 1926 reactions of 602 closed shell and free radical species, which treat the chemistry initiated by reaction with OH radicals,
NO$_3$ radicals and ozone. It contains much of the isoprene HO$_X$ recycling chemistry identified as important in recent years

270 under "low NO" conditions, including the peroxy radical 1,4 and 1,6 H-shift chemistry described in the LIM1 mechanism

(Peeters et al., 2009; 2014), as summarized in Wennberg et al. (2018). Model photolysis rates were calculated using the Tropospheric Ultraviolet and Visible Radiation Model (TUV v5.2) (Madronich, 1993).

The box model was initialised with a range of different concentrations of isoprene (1.7 ppb, 3.4 ppb, 5.0 ppb, 6.7 ppb), and OH (0.25, 0.5, 1.0, 3.0, 10, 20 × 10^6 cm^{-3}). [CH$_4$] was fixed at 1.85 ppmv and [CO] at 110 ppbv, and T = 298 K. Entrainment

275 loss rates for all model species were set to 1 × 10^{-5} cm^{-3} s^{-1}. For the box model, a column average value for deposition velocity, V_d, was calculated according to the functionalities of each species (Table S2). These terms prevent the build-up of secondary products. The values are based on reported deposition rates in Nguyen et al. (2015). A boundary layer height (*BLH*) of 1.5 km was assumed. Loss rates (*L$_d$*) for each species to dry deposition are then $L_d = V_d/BLH$. Photolysis rates were fixed to mean rates for the day time period 09:00-17:00 calculated for July 1. The model was then run to steady state for a range of fixed NO

280 mixing ratios from 0 – 16,000 pptv.

Data availability

Data are available at http://catalogue.ceda. ac.uk/uuid/7ed9d8a288814b8b85433b0d3fec0300 (last access: 13 Feb 2020). Specific data are available from the authors on request (jacqui.hamilton@york.ac.uk).

Author Contributions

285 JRH, RED, JFH, WJFA, CNH, BL and XW provided the VOC measurements. FAS, WSD and JDL provided the NO$_x$ and O$_3$ measurements. TJB, AM, SDW, AB, CJP and HC collected and analysed the CIMS data. TQ and JDS provided the organo-sulfate standards. DB, WD and JFH provided the organo-sulfate aerosol measurements. LKW, DEH, EJS, RW-M and CY provided the OH and HO$_2$ data. MN, PME and ARR provided the MCM box modelling. PDI and MJE provided the GEOS-Chem model run. ACL is the PI of the AIRPRO-Beijing project. MJN, JFH and ARR conceived and wrote the manuscript

290 with input and discussion with all co-authors.

Competing Interests

The authors declare that they have no conflict of interest.

Acknowledgements

This project was funded by the Natural Environment Research Council, the Newton Fund and Medical Research Council in

295 the UK, and the National Natural Science Foundation of China (NE/N007190/1, NE/N006917/1). We acknowledge the support from Pingqing Fu, Zifa Wang, Jie Li and Yele Sun from IAP for hosting the APHH-Beijing campaign at IAP. We thank Zongbo Shi, Roy Harrison, Tuan Vu and Bill Bloss from the University of Birmingham, Siyao Yue, Liangfang Wei, Hong

Ren, Qiaorong Xie, Wanyu Zhao, Linjie Li, Ping Li, Shengjie Hou, Qingqing Wang from IAP, Kebin He and Xiaoting Cheng from Tsinghua University, and James Allan from the University of Manchester for providing logistic and scientific support for the field campaigns.

300

References

Air Quality Expert Group: Ozone in the United Kingdom, Department for the Environment, Food and Rural Affairs, http://www.defra.gov.uk/environment/airquality/aqeg, 2009.

305   Bannan, T. J., Booth, A. M., Bacak, A., Muller, J. B. A., Leather, K. E., Le Breton, M., Jones, B., Young, D., Coe, H., Allan, J., Visser, S., Slowik, J. G., Furger, M., Prevot, A. S. H., Lee, J. Dunmore, R. E., Hopkins, J. R., Hamilton, J. F., Lewis, A. C., Whalley, L. K., Sharp, T., Stone, D., Heard, D. E., Fleming, Z. L., Leigh, R., Shallcross, D. E., and Percival, C. J.: The first U.K. measurements of nitryl chloride using a chemical ionisation mass spectrometer in London, ClearfLo Summer, 2012, and an investigation of the role of Cl atom oxidation. Journal of Geophysical Research, 120, 5638-5657, 2015.

310

Bannan, T. J., Le Breton, M., Priestley, M., Worrall, S. D., Bacak, A., Marsden, N. A., Mehra, A., Hammes, J., Hallquist, M., Alfarra, M. R., Krieger, U. K., Reid, J. P., Jayne, J., Robinson, W., McFiggans, G., Coe, H., Percival, C. J., and Topping, D.: A method for extracting calibrated volatility information from the FIGAERO-HR-ToF-CIMS and its experimental application, Atmos. Meas. Tech., 12, 1429–1439, https://doi.org/10.5194/amt-12-1429-2019, 2019.

315

Bianchi F., Kurtén, T., Riva, M., Mohr, C., Rissanen, M. P., Roldin, P., Berndt, T., Crounse, J. D., Wennberg, P. O., Mentel, T. F., Wildt, J., Junninen, H., Jokinen, T., Kulmala, M., Worsnop, D. R., Thornton, J. A., Donahue, N. Kjaergaard, H. G., and Ehn, M.: Highly Oxygenated Organic Molecules (HOM) from Gas-Phase Autoxidation Involving Peroxy Radicals: A Key Contributor to Atmospheric Aerosol, Chem. Rev., 119, 3472-3509, 2019.

320

Brean, J., Harrison, R. M., Shi, Z., Beddows, D. C. S., Acton, W. J. F., Hewitt, C. N., Squires, F. A., and Lee, J.: Observations of highly oxidized molecules and particle nucleation in the atmosphere of Beijing, Atmos. Chem. Phys., 19, 14933–14947, https://doi.org/10.5194/acp-19-14933-2019, 2019.

325   Bryant, D. J., Dixon, W. J., Hopkins, J. R., Dunmore, R. E., Pereira, K. L., Shaw, M., Squires, F. A., Bannan, T. J., Mehra, A., Worrall, S. D., Bacak, A., Coe, H., Percival, C. J., Whalley, L. K., Heard, D. E., Slater, E. J., Ouyang, B., Cui, T., Surratt, J. D., Liu, D., Shi, Z., Harrison, R., Sun, Y., Xu, W., Lewis, A. C., Lee, J. D., Rickard, A. R., and Hamilton, J. F.: Strong anthropogenic control of secondary organic aerosol formation from isoprene in Beijing, Atmos. Chem. Phys. Discuss., https://doi.org/10.5194/acp-2019-929, in review, 2019.

330

Chan, A. W. H., Chan, M. N., Surratt, J. D., Chhabra, P. S., Loza, C. L., Crounse, J. D., Yee, L. D., Flagan, R. C., Wennberg, P. O., and Seinfeld, J. H.: Role of aldehyde chemistry and NO_x concentrations in secondary organic aerosol formation, Atmos. Chem. Phys., 10, 7169–7188, https://doi.org/10.5194/acp-10-7169-2010, 2010.

335 Commane, R., Floquet, C. F. A., Ingham, T., Stone, D., Evans, M. J., and Heard, D. E.: Observations of OH and HO_2 radicals over West Africa, Atmos. Chem. Phys., 10, 8783–8801, https://doi.org/10.5194/acp-10-8783-2010, 2010.

Crounse, J. D., Nielsen, L. B., Jørgensen, S., Kjaergaard, H. G., and Wennberg, P.: Autooxidation of Organic Compounds in the Atmosphere, J. Phys. Chem. Lett., 4, 3513-3520, 2013.

340

Emmerson, K. M., and Evans, M. J.: Comparison of tropospheric gas-phase chemistry schemes for use within global models, Atmos. Chem. Phys., 9, 1831-1845, https://doi.org/10.5194/acp-9-1831-2009, 2009.

Hamilton, J. F., Lewis, A.C., Carey, T. J., and Wenger, J. C.: Characterization of Polar Compounds and Oligomers in 345 Secondary Organic Aerosol Using Liquid Chromatography Coupled to Mass Spectrometry, Anal. Chem., 80, 474-480, 2008.

Hopkins, J. R., Jones, C. E., and Lewis, A. C.: A dual channel gas chromatograph for atmospheric analysis of volatile organic compounds including oxygenated and monoterpene compounds, J. Environ. Monit., 13, 2268-2276, 2011.

350 Jenkin, M. E., Saunders, S. M., and Pilling, M. J.: The tropospheric degradation of volatile organic compounds: a protocol for mechanism development, Atmos. Environ., 31, 81–104, 1997.

Jenkin, M. E., Young, J. C., and Rickard, A. R. R.: The MCM v3.3.1 degradation scheme for isoprene, Atmos. Chem. Phys., 15, 11433-11459, 2015.Hofzumahaus, A., Rohrer, F., Lu, K., et al.: Amplified Trace Gas Removal in the Troposphere, Science, 355 324, 1702-1704, 2009.

Jimenez, J. L., Canagaratna, M. R., Donahue, Prevot, A. S. H., Zhang, Q., Kroll, J. H. DeCarlo, P. F., Allan, J. D., Coe, H., Ng, N. L., Aiken, A. C., Docherty, K. S., Ulbrich, I. M., Grieshop, A. P., Robinson, A. L., Duplissy, J., Smith, J. D., Wilson, K. R., Lanz, V. A., Hueglin, C., Sun, Y. L., Tian, J., Laaksonen, A., Raatikainen, T., Rautiainen, J., Vaattovaara, P., Ehn, M., 360 Kulmala, M., Tomlinson, J. M., Collins, D. R., Cubison, M. J., Dunlea, E. J., Huffman, J. A., Onasch, T. B., Alfarra, M. R., Williams, P. I., Bower, K., Kondo, Y., Schneider, J., Drewnick, F., Borrmann, S., Weimer, S., Demerjian, K., Salcedo, D., Cottrell, L., Griffin, R., Takami, A., Miyoshi, T., Hatakeyama, S., Shimono, A., Sun, J. Y., Zhang, Y. M., Dzepina, K., Kimmel,

J. R., Sueper, D., Jayne, J. T., Herndon, S. C., Trimborn, A. M., Williams, L. R., Wood, E. C.. Middlebrook, A. M., Kolb, C. E., Baltensperger, U., and Worsnop, D. R.: Evolution of Organic Aerosols in the Atmosphere, Science, 326, 1525-1529, 2009.

365

Jordan, A., Haidacher, S., Hanel, G., Hartungen, E., Märk, L., Seehauser, H., Schottkowsky, R., Sulzer, P., and Märk T.D.: A high resolution and high sensitivity proton-transfer-reaction time-of-flight mass spectrometer (PTR-TOF-MS), Int. J. Mass Spectrom., 286, 122-128, 2009.

370   Kroll, J. H., Ng, N. L., Murphy, S. M., Flagan, R. C., and Seinfeld, J. H.: Secondary organic aerosol formation from isoprene photooxidation, Environ. Sci. Technol., 40, 1869–1877, 2006.

Le Breton, M., Wang, Y., Hallquist, Å. M., Pathak, R. K., Zheng, J., Yang, Y., Shang, D., Glasius, M., Bannan, T. J., Liu, Q., Chan, C. K., Percival, C. J., Zhu, W., Lou, S., Topping, D., Wang, Y., Yu, J., Lu, K., Guo, S., Hu, M., and Hallquist, M.:
375   Online gas- and particle-phase measurements of organosulfates, organosulfonates and nitrooxy organosulfates in Beijing utilizing a FIGAERO ToF-CIMS, Atmos. Chem. Phys., 18, 10355-10371, https://doi.org/10.5194/acp-18-10355-2018, 2018.

Lee, B. H., Lopez-Hilfiker, F. D., Mohr, C., Kurtén, T., Worsnop, D. R., and Thornton, J. A.: An iodide-adduct high-resolution time-of-flight chemical-ionization mass spectrometer: Application to atmospheric inorganic and organic compounds, Environ.
380   Sci. Technol., 48, 6309-6317, 2014.

Li, K., Jacob, D. J., Liao, H., Shen, L., Zhang, Q., and Bates, K. H.: Anthropogenic drivers of 2013-2017 trends in summer surface ozone in China, Proc. Natl. Acad. Sci., 116, 422-427, 2019.

385   Lin, Y-H., Zhang, Z., Docherty, K. S., Zhang, H., Budisulistiorini, S. H., Rubitschin, C. L., Shaw, S. L., Knipping, E. M., Edgerton, E. S., Kleindienst, T. E., Gold, A., Surratt, J. D.: Isoprene Epoxydiols as Precursors to Secondary Organic Aerosol Formation: Acid-Catalyzed Reactive Uptake Studies with Authentic Compounds, Environ. Sci. Technol., 46, 250-258, 2012.

Lopez-Hilfiker, F. D., Mohr, C., Ehn, M., Rubach, F., Kleist, E., Wildt, J., Mentel, Th. F., Lutz, A., Hallquist, M., Worsnop,
390   D., and Thornton, J. A.: A novel method for online analysis of gas and particle composition: description and evaluation of a Filter Inlet for Gases and AEROsols (FIGAERO), Atmos. Meas. Tech., 7, 983–1001, https://doi.org/10.5194/amt-7-983-2014, 2014.

Madronich, S.: The Atmosphere and UV-B Radiation at Ground Level. In: Young, A. R., Moan, J., Björn, L. O., Nultsch, W.,
395   editors. Environmental UV Photobiology. Boston, MA, Springer US, pp. 1-39., 1993.

Nguyen, T. B., Crounse, J. D., Teng, A. P., Clair, J. M. S., Paulot, F., Wolfe, G. M., and Wennberg, P. O.: Rapid deposition of oxidized biogenic compounds to a temperate forest, Proc. Natl. Acad. Sci., 112, E392-E401, 2015.

400   Nguyen, T. B., Bates, K. H., Crounse, J. D., Schwantes, R. H., Zhang, X., Kjaergaard, H. G., Surratt, J. D., Lin, P., Laskin, A., Seinfeld, J. H., and Wennberg, P. O.: Mechanism of the hydroxyl radical oxidation of methacryloyl peroxynitrate (MPAN) and its pathway toward secondary organic aerosol formation in the atmosphere, Phys. Chem. Chem. Phys., 17, 17914–17926, https://doi.org/10.1039/C5CP02001H, 2015.

405   Orlando, J. J., and Tyndall, G. S.: Laboratory studies of organic peroxy radical chemistry: an overview with emphasis on recent issues of atmospheric significance, Chem. Soc. Rev., 41, 6294-6317, 2012.

Paulot, F., Crounse, J. D., Kjaergaard, H. G., Kürten, A., St. Clair, J. M., Seinfeld, J. H., and Wennberg, P. O.: Unexpected epoxide formation in the gas-phase photooxidation of isoprene, Science, 325, 730-733, 2009.

410

Peeters, J., Nguyen, T. L., and Vereecken, L.: HOx radical regeneration in the oxidation of isoprene, Phys. Chem. Chem. Phys., 11, 5935-5939, 2009.

Peeters, J., Müller, J. -F., Stavrakou, T., and Nguyen, V. S.: Hydroxyl Radical Recycling in Isoprene Oxidation Driven by
415   Hydrogen Bonding and Hydrogen Tunneling: The Upgraded LIM1 Mechanism, J. Phys. Chem. A., 118, 8625-8643, 2014.

Priestley, M., Le Breton, M., Bannan, T. J., Leather, K. E., Bacak, A., Reyes-Villegas, E., de Vocht, F., Shallcross, B. M. A., Brazier, T., Khan, M. A., Allan, J., Shallcross, D. E., Coe, H., Percival, C. J.: Observations of isocyanate, amide, nitrate and nitro compounds from an anthropogenic biomass burning event using a ToF-CIMS, J Geophys. Res. Atmos., 123, 7687-7704,
420   2018.

Ren, X., Harder, H., Martinez, M., Lesher, R. L., Oliger, A., Simpas, J. B., Brune, W. H., Schwab, J. J., Demerjian, K. L., He, Y., Zhou, X., and Gao, H.: OH and HO_2 chemistry in the urban atmosphere of New York City, Atmos. Environ., 37, 3639–3651, 2003.

425

Rivera-Rios, J. C., Nguyen, T. B., Crounse, J. D., Jud, W., St. Clair, J. M., Mikoviny, T., Gilman, J. B., Lerner, B. M., Kaiser, J. B., de Gouw, J., Wisthaler, A., Hansel, A., Wennberg, P. O., Seinfeld, J. H., and Keutsch, F. N.: Conversion of hydroperoxides to carbonyls in field and laboratory instrumentation: Observational bias in diagnosing pristine versus anthropogenically controlled atmospheric chemistry, Geophys. Res. Lett., 41, 8645–8651, doi:10.1002/ 2014GL061919, 2014.

430

Sanchez, D., Jeong, D., Seco, R., Wrangham, I., Park, J. H., Brune, W. H., Koss, A., Gilman, J., de Gouw, J., Misztal, P., Goldstein, A., Baumann, K., Wennberg, P. O., Keutsch, F. N., Guenther, A., and Kim. S.: Intercomparison of OH and OH reactivity measurements in a high isoprene and low NO environment during the Southern Oxidant and Aerosol Study (SOAS), Atmos. Environ., 174, 227-236, 2018.

435

Schwantes, R. H., Charan, S. M., Bates, K. H., Huang, Y., Nguyen, T. B., Mai, H., Kong, W., Flagan, R. C., and Seinfeld, J. H.: Low-volatility compounds contribute significantly to isoprene secondary organic aerosol (SOA) under high-NO_x conditions, Atmos. Chem. Phys., 19, 7255–7278, https://doi.org/10.5194/acp-19-7255-2019, 2019.

440 Shi, Z., Vu, T., Kotthaus, S., Harrison, R. M., Grimmond, S., Yue, S., Zhu, T., Lee, J., Han, Y., Demuzere, M., Dunmore, R. E., Ren, L., Liu, D., Wang, Y., Wild, O., Allan, J., Acton, W. J., Barlow, J., Barratt, B., Beddows, D., Bloss, W. J., Calzolai, G., Carruthers, D., Carslaw, D. C., Chan, Q., Chatzidiakou, L., Chen, Y., Crilley, L., Coe, H., Dai, T., Doherty, R., Duan, F., Fu, P., Ge, B., Ge, M., Guan, D., Hamilton, J. F., He, K., Heal, M., Heard, D., Hewitt, C. N., Hollaway, M., Hu, M., Ji, D., Jiang, X., Jones, R., Kalberer, M., Kelly, F. J., Kramer, L., Langford, B., Lin, C., Lewis, A. C., Li, J., Li, W., Liu, H., Liu, J., 445 Loh, M., Lu, K., Lucarelli, F., Mann, G., McFiggans, G., Miller, M. R., Mills, G., Monk, P., Nemitz, E., O'Connor, F., Ouyang, B., Palmer, P. I., Percival, C., Popoola, O., Reeves, C., Rickard, A. R., Shao, L., Shi, G., Spracklen, D., Stevenson, D., Sun, Y., Sun, Z., Tao, S., Tong, S., Wang, Q., Wang, W., Wang, X., Wang, X., Wang, Z., Wei, L., Whalley, L., Wu, X., Wu, Z., Xie, P., Yang, F., Zhang, Q., Zhang, Y., Zhang, Y., and Zheng, M.: Introduction to the special issue "In-depth study of air pollution sources and processes within Beijing and its surrounding region (APHH-Beijing)", Atmos. Chem. Phys., 19, 7519– 450 7546, https://doi.org/10.5194/acp-19-7519-2019, 2019.

Sindelarova, K., Granier, C., Bouarar, I., Guenther, A., Tilmes, S., Stavrakou, T., Müller, J.-F., Kuhn, U., Stefani, P., and Knorr, W.: Global data set of biogenic VOC emissions calculated by the MEGAN model over the last 30 years, Atmos. Chem. Phys., 14, 9317-9341, https://doi.org/10.5194/acp-14-9317-2014, 2014.

455

Stone, D., Whalley, L. K., Ingham, T., Edwards, P. M., Cryer, D. R., Brumby, C. A., Seakins, P. W., and Heard, D. E.: Measurement of OH reactivity by laser flash photolysis coupled with laser-induced fluorescence spectroscopy, Atmos. Meas. Tech., 9, 2827–2844, https://doi.org/10.5194/amt-9-2827-2016, 2016.

460 Surratt, J. D., Murphy, S. M., Kroll, J. H., Ng, N. L., Hildebrandt, L., Sorooshian, A., Szmigielski, R., Vermeylen, R., Maenhaut, W., Claeys, M., Flagan, R. C., and Seinfeld, J. H.: Chemical composition of secondary organic aerosol formed from the photooxidation of isoprene, J. Phys. Chem. A., 110, 9665–9690, 2006.

Surratt, J. D., Chan, A. W. H., Eddingsaas, N. C., Chan, M. N., Loza, C. L., Kwan, A. J., Hersey, S. P., Flagan, R. C., Wennberg,
P. O., and Seinfeld, J. H.: Reactive intermediates revealed in secondary organic aerosol formation from isoprene, Proc. Natl.
Acad. Sci., 107, 6640-6645, 2010.

Tan, Z., Lu, K., Hofzumahaus, A.: Experimental budgets of OH, HO$_2$, and RO$_2$ radicals and implications for ozone formation
in the Pearl River Delta in China 2014, Atmos. Chem. Phys., 19, 7129-7150, 2019.

Wennberg, P. O., Bates, K. H., Crounse, J. D., Dodson, L. G., McVay, R. C., Mertens, L. A., Nguyen, T. B., Praske, E.,
Schwantes, R. H., Smarte, M. D., St. Clair, J. M., Teng, A. P., Zhang, X., and Seinfeld J. H.: Gas-phase reactions of isoprene
and its major oxidation products, Chem. Rev., 118, 3337-3390, 2018.

Whalley, L. K., Edwards, P. M., Furneaux, K. L., Goddard, A., Ingham, T., Evans, M. J., Stone, D., Hopkins, J. R., Jones, C.
E., Karunaharan, A., Lee, J. D., Lewis, A. C., Monks, P. S., Moller, S. J., and Heard, D. E.: Quantifying the magnitude of a
missing hydroxyl radical source in a tropical rainforest, Atmos. Chem. Phys., 11, 7223-7233, https://doi.org/10.5194/acp-11-
7223-2011, 2011.

Whalley, L. K., Stone, D., Bandy, B., Dunmore, R., Hamilton, J. F., Hopkins, J., Lee, J. D., Lewis, A. C., and Heard, D. E.:
Atmospheric OH reactivity in central London: observations, model predictions and estimates of in situ ozone production,
Atmos. Chem. Phys., 16, 2109-2122, https://doi.org/10.5194/acp-16-2109-2016, 2016.

Whalley, L. K., Stone, D., Dunmore, R., Hamilton, J., Hopkins, J. R., Lee, J. D., Lewis, A. C., Williams, P., Kleffmann, J.,
Laufs, S., Woodward-Massey, R., and Heard, D. E.: Understanding in situ ozone production in the summertime through radical
observations and modelling studies during the Clean air for London project (ClearfLo), Atmos. Chem. Phys., 18, 2547-2571,
https://doi.org/10.5194/acp-18-2547-2018, 2018.

Woodward-Massey, R.: Observations of radicals in the atmosphere: measurement validation and model comparisons, PhD
Thesis, University of Leeds, 2018.

Zhou, W., Zhao, J., Ouyang, B., Mehra, A., Xu, W., Wang, Y., Bannan, T. J., Worrall, S. D., Priestley, M., Bacak, A., Chen,
Q., Xie, C., Wang, Q., Wang, J., Du, W., Zhang, Y., Ge, X., Ye, P., Lee, J. D., Fu, P., Wang, Z., Worsnop, D., Jones, R.,
Percival, C. J., Coe, H., and Sun, Y.: Production of N2O5 and ClNO2 in summer in urban Beijing, China, Atmos. Chem. Phys.,
18, 11581-11597, https://doi.org/10.5194/acp-18-11581-2018, 2018.
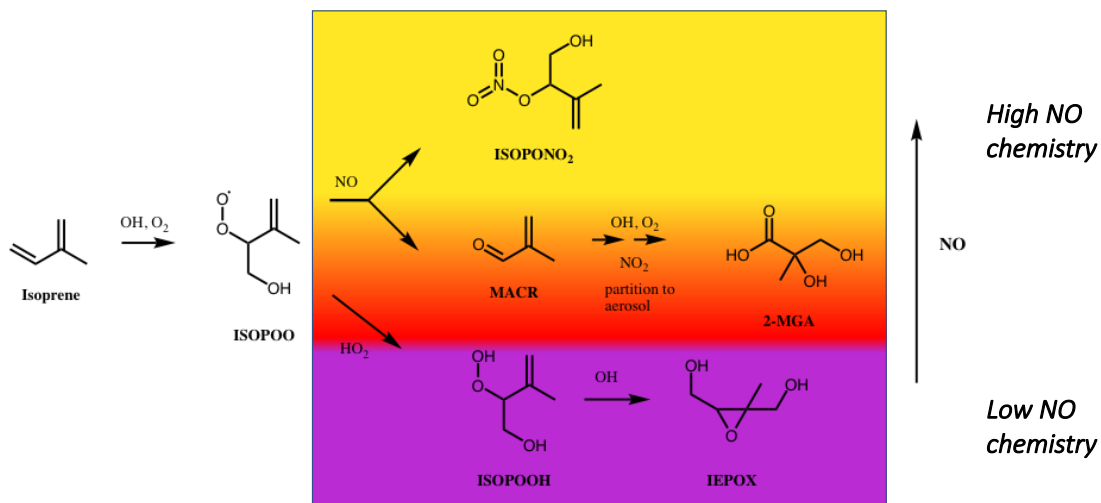
Figure 1: Formation pathways of isoprene oxidation products used as tracers of high / low-NO chemistry in this work. Following reaction of the primary VOC, isoprene, with OH, a peroxy radical intermediate (ISOPOO) is formed. At low NO concentrations, ISOPOO reacts with HO2 (or other RO2), to yield hydroperoxide (ISOPOOH) isomers ((4,3)-ISOPOOH isomer is shown), which can be rapidly oxidized to isoprene epoxydiol (IEPOX) isomers. At high NO concentrations, ISOPOO reacts with NO, a minor product of which is an isoprene nitrate (ISOPONO2). One of the major products of ISOPOO reaction with NO is methacrolein (MACR), the subsequent oxidation of which, in the presence of NO2, can lead to 2-methylglyceric acid (2-MGA) and its corresponding oligomers and organosulfates in the aerosol phase. Measurements of these products in the gas or aerosol phase can be used as tracers for the chemical environment in which they were formed.

500

505

510
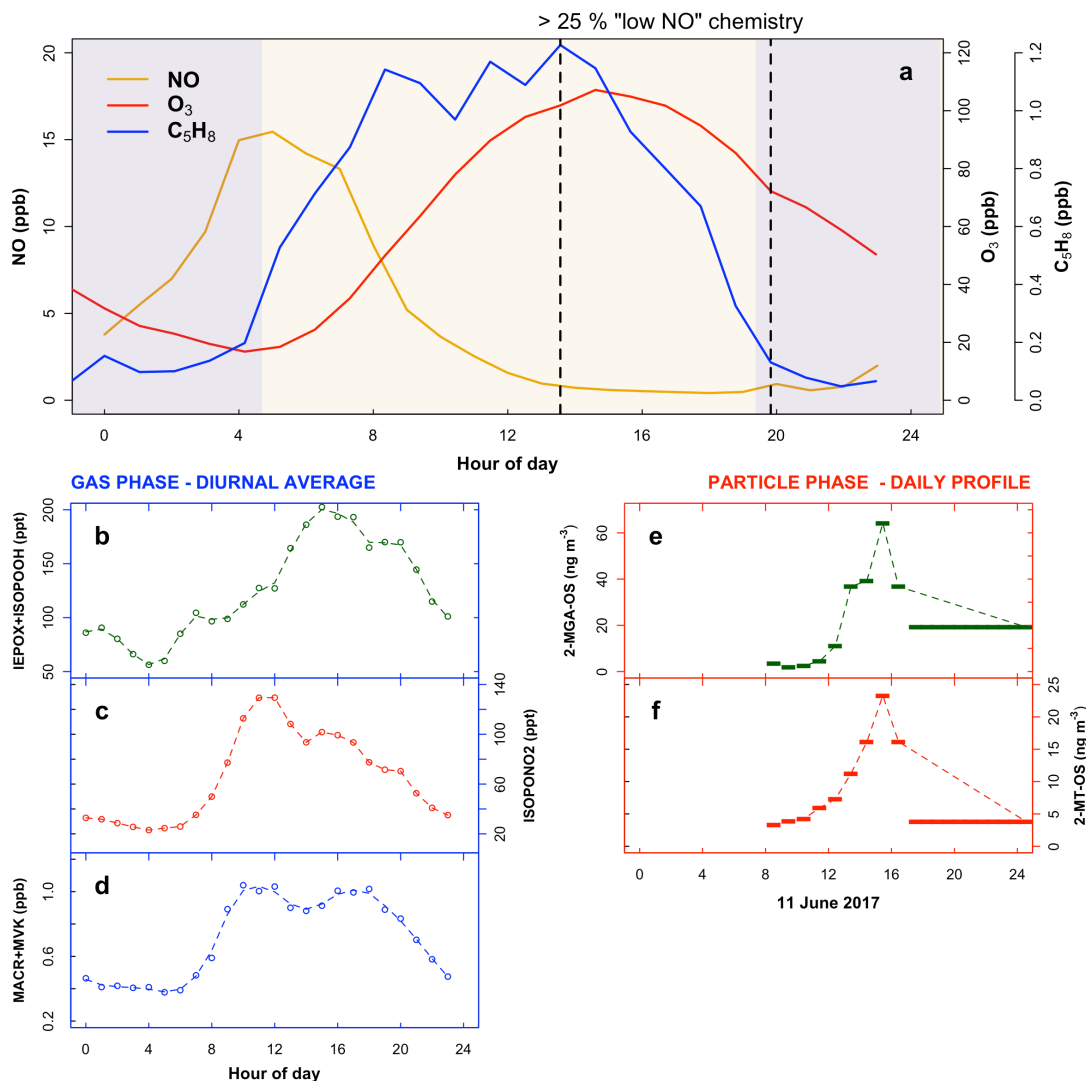
Figure 2: Mean diurnal variation of measured organic and inorganic species in the gas phase and aerosol during the Beijing summer observations. a. Mean diurnal cycle of the inorganic species NO and ozone (O3) and of the product precursor isoprene (C5H8). Shaded areas are at night; area between the dotted lines indicates where > 25% of the isoprene chemistry is driven by low NO pathways (Fig. 3). b&c. Mean diurnal cycle of the gas phase isoprene 'low NO' oxidation products, IEPOX + ISOPOOH (b), and 'high NO' oxidation product, isoprene nitrate (ISOPONO2) (c). d. Mean diurnal cycle of the gas phase isoprene oxidation products methacrolein (MACR) (precursor to 2-MGA) + methyl vinyl ketone (MVK). e&f. SOA components: 2-methyltetrol-organosulfate (2-MT-OS) and 2-methylglyceric acid-organosulfate (2-MGA-OS), both measured on the 11/12th June 2017, the last filter sample was taken from 17:30 11 June - 08:30 12 June.
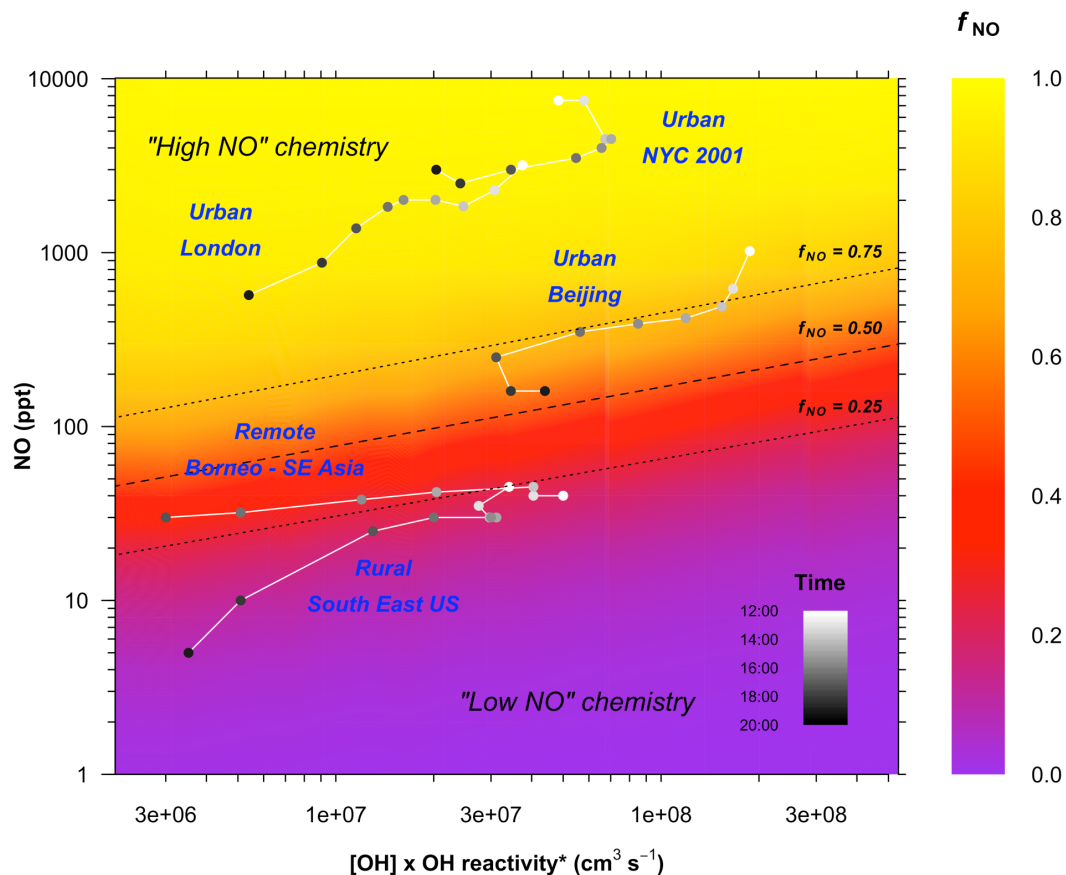
Figure 3: Variation of the fraction of ISOPOO reacting with NO as a function of NO concentration and the reactivity of the system. The plot is derived from a series of zero-dimensional box model runs performed as a function of fixed concentrations of [NO], [OH], and [isoprene]. Photolysis is fixed to an average of 09:00-17:00 conditions. OH reactivity* is total OH reactivity of the chemical system minus the contribution from OH + NOx (Equation E1), since these reactions do not produce RO2.

$$\text{OH reactivity*} = \sum k_{OH+VOC}[\text{VOC}] \quad (E1)$$

The dashed line shows the fraction of ISOPOO reacting with NO $f_{NO} = 0.50$, dotted lines show $f_{NO} = 0.25$ and 0.75. Points are average diurnal hourly measurements of NO, OH, and OH reactivity* for the period 12:00 – 20:00 pm from a range of different environments: The rural sites, Borneo (Whalley et al., 2011) (only shown for 12:00-18:00) and the Southeast US (Sanchez et al., 2018), and the urban sites London (Whalley et al., 2016), New York City (Ren et al., 2003), and Beijing (this work). See the SI for full details.